

Check for updates

The Electrochemical Acetone/Isopropanol Hydrogenation Cycle – An Alternative to Current Hydrogen Storage Solutions

Dominik Venus,* Axel Marth,* Sebastian Riess, Anna T.S. Freiberg, Matthew Brodt, Michael Wensing, Peter Wasserscheid, and Simon Thiele*

Liquid organic hydrogen carrier (LOHC) systems offer a promising way to store hydrogen using the existing infrastructure for liquid fuels. While LOHC hydrogenation and dehydrogenation processes have so far mainly been investigated using thermocatalytic processes, this work explores the concept of a low-temperature (<80 °C) electrochemical acetone/isopropanol LOHC cycle and indicates its potential benefits for a future hydrogen economy. This electrochemical liquid organic hydrogen carrier (EC-LOHC) system builds on low-cost chemicals with low ecotoxicology. In this study, the influence of temperature and fuel concentrations on the polarization curves of the electrochemical hydrogenation and dehydrogenation units in a small, single-cell set-up is investigated using proton exchange membrane fuel cell components. Based on the experimental results, efficiencies are determined for a power-to-power cycle that can be competitive to mature hydrogen storage technologies, such as liquid and compressed hydrogen storage. Finally, material-related challenges are discussed, encouraging future research in this new field of hydrogen storage.

D. Venus, A. Marth, A. T. Freiberg, M. Brodt, P. Wasserscheid, S. Thiele Forschungszentrum Jülich GmbH
Helmholtz-Institute Erlangen-Nürnberg (HI ERN)
91058 Erlangen, Germany
E-mail: do.venus@fz-juelich.de; a.marth@fz-juelich.de;
s.thiele@fz-juelich.de

D. Venus, A. Marth, A. T. Freiberg, P. Wasserscheid, S. Thiele Department Chemical and Biological Engineering Friedrich-Alexander-Universität Erlangen-Nürnberg 91058 Erlangen, Germany S. Riess, M. Wensing

S. Riess, M. Wensing
Fluid Systems Technology
Friedrich-Alexander-Universität Erlangen-Nürnberg
91058 Erlangen, Germany
P. Wasserscheid
Institute for a Sustainable Hydrogen Economy
Forschungszentrum Jülich GmbH
52428 Jülich, Germany

The ORCID identification number(s) for the author(s) of this article can be found under https://doi.org/10.1002/aenm.202403824

© 2024 The Author(s). Advanced Energy Materials published by Wiley-VCH GmbH. This is an open access article under the terms of the Creative Commons Attribution License, which permits use, distribution and reproduction in any medium, provided the original work is properly cited.

DOI: 10.1002/aenm.202403824

1. Introduction

Green hydrogen from renewable energybased water electrolysis is widely considered to become a key factor in decarbonizing the energy and chemical industries. The conversion of electric energy into chemical energy stored in a hydrogen carrier opens an enormous potential for storing fluctuating excess wind and solar energy for later use on demand. Storing hydrogen, however, is an arduous process. While hydrogen has an excellent gravimetric energy density (33.33 kWh kg_{H2}⁻¹ based on the lower heating value (LHV)), it is also characterized by a low volumetric energy density at ambient conditions (3 Wh L^{-1}), which requires technical measures to increase its volumetric energy density for storage.^[1] The most commonly used commercial hydrogen storage methods

are compressed hydrogen (CH₂ at 350 or 700 bar) and liquefied hydrogen (LH₂ at -253 °C and ambient pressure). Detailed approaches store hydrogen in its molecular state. Additionally, hydrogen storage in liquid organic hydrogen carriers (LOHC) has drawn significant attention over the past decade. LOHC systems consist of a hydrogen-lean compound (LOHC-) and a hydrogen-rich compound (LOHC+) that can be reversibly converted into each other by thermocatalytic hydrogenation/dehydrogenation cycles that can store and release hydrogen on demand. As shown in Figure 1, the different options for hydrogen storage vary considerably in their respective storage efficiencies and conceptual advantages.

The outstanding advantages of liquid hydrogen carriers are high volumetric energy densities, facile handling, and storage without losses within existing fuel infrastructures. Methanol (5.47 kWh kg $^{-1}$ / 4.33 kWh L $^{-1}$ based on LHV $_{\rm MeOH}$) and liquid ammonia (4.81 kWh kg $^{-1}$ / 3.28 kWh L $^{-1}$ based on LHV $_{\rm NH3}$) are among the best-known liquid hydrogen carriers. [11–14]

However, methanol and ammonia are chemicals with high acute toxicity obtained in strongly equilibrium-restricted, high-pressure hydrogenation processes that require expensive process equipment and are difficult to operate economically in decentralized scenarios. [4,15] Moreover, green industrial-scale ${\rm CO}_2$ reduction to methanol would require carbon capture, another

16146840, 2025, 12, Downloaded from https://advanced.onlinelibrary.wiley.com/doi/10.1002/aenm.202403824 by Forschungszentrum Jülich GmbH Research Center, Wiley Online Library on [09/042025]. See the Terms and Conditions (https://onlinelibrary.wiley

on Wiley Online Library for rules of use; OA articles are governed by the applicable Creative Commons!

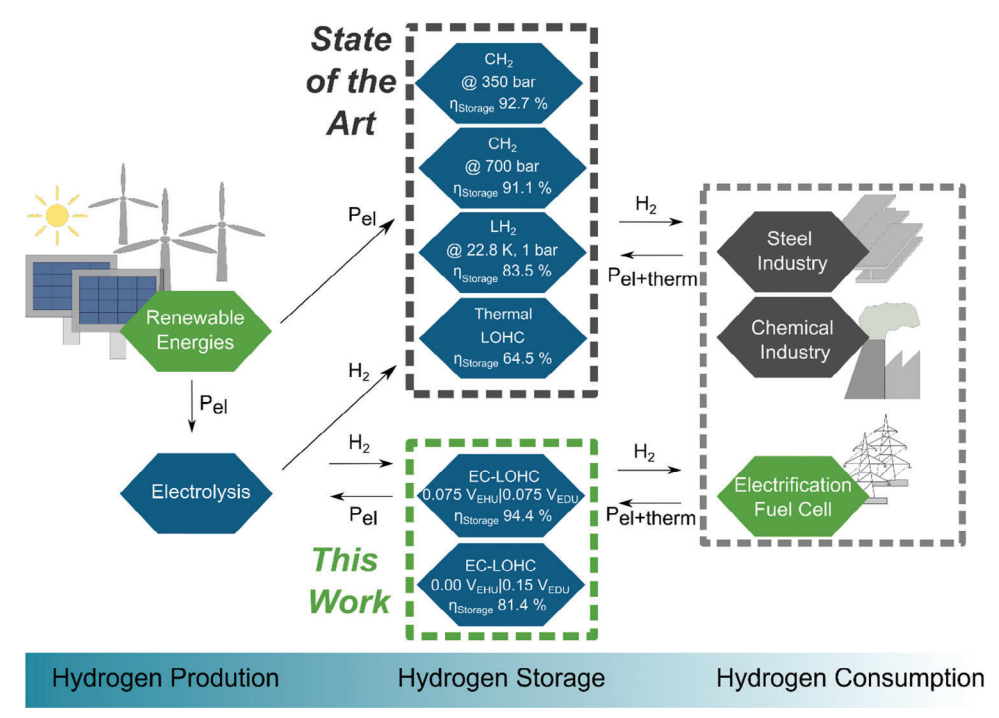


Figure 1. Hydrogen economy with production, storage and consumption including hydrogen and energy fluxes. Different existing storage technologies and their efficiencies are compared to the novel concept of an electrochemical hydrogen storage investigated in this work. The corresponding storage efficiencies are calculated according to Equation (2) and are also depicted in Table 1 and Figure 9.

expensive process that is still in its development stage. ^[16] Consequently, liquid, reversible, CO₂-free, and safe energy storage systems are highly desired.

Thermocatalytic LOHC-based hydrogen storage technologies that are already commercially available use toluene/methylcyclohexane (TOL/MCH), $\rm H_0\text{-}DBT/H_{18}\text{-}DBT$, or $\rm H_0\text{-}BT/H_{12}\text{-}BT$ as their corresponding LOHC- and LOHC+ compounds. However, hydrogen release from MCH, $\rm H_{18}\text{-}DBT$, and $\rm H_{12}\text{-}BT$ at hydrogen partial pressures above 1 bar requires temperatures exceeding 250 °C. $^{[4-6]}$ Among these LOHC systems, only for TOL/MCH, an electrochemical hydrogenation at low temperatures has been described. $^{[17]}$ However, there is great interest in electrochemical addressable LOHC systems as electrochemical processes are advantageous regarding flexible operation, device size, scalability, and system simplicity. $^{[18]}$ These are essential process advantages when storing fluctuating wind and solar energy.

In search of suitable electrochemical, liquid organic hydrogen carriers (EC-LOHC), the following properties are highly beneficial: a) Water solubility of the EC-LOHC- and EC-LOHC+ compounds to access established aqueous electrochemistry; b) At least one functional group of the EC-LOHC-/EC-LOHC+ compounds should be accessible to reversible hydrogenation/dehydrogenation without breaking C-C bonds to avoid CO₂ formation.

Under these selection criteria, ketones/secondary alcohols are promising EC-LOHC systems as they can be selectively reduced and oxidized in closed-loop storage cycles.^[19] In contrast to primary alcohols, secondary alcohol functionalities can be dehydrogenated without breaking any C-C bond.^[20,21]

The simplest ketone/secondary alcohol pair is acetone (ACE) and isopropanol (2-propanol, IPA). Acetone and isopropanol are biodegradable, low-toxic, liquid at ambient conditions, readily available in large volumes at low cost, and can be easily stored in existing low-cost tank equipment.^[22,23] Acetone can be reduced to isopropanol in a system that we denote as an electrochemical hydrogenation unit (EHU) (**Figure 2a**). The two half-cell reactions are the anodic hydrogen oxidation reaction (HOR) and

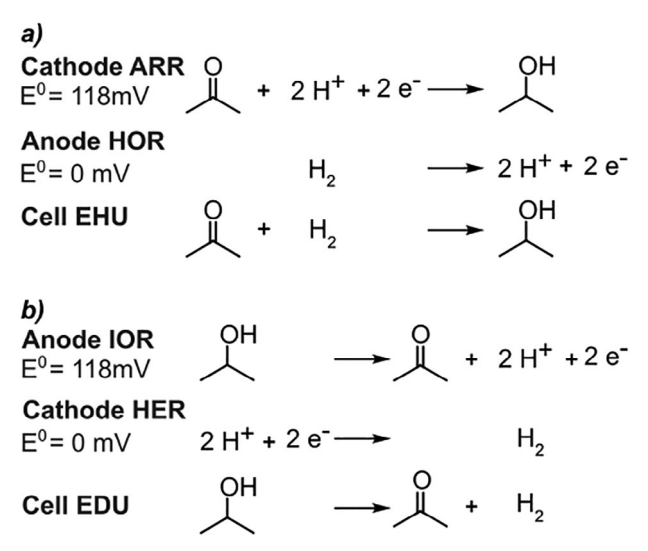


Figure 2. Reaction equations in acidic environments and standard reaction potentials (E^0) for a) the electrochemical hydrogenation of acetone and b) the electrochemical dehydrogenation of isopropanol.



ADVANCED ENERGY MATERIALS

www.advenergymat.de

the cathodic acetone reduction reaction (ARR). Subsequently, the electrochemical dehydrogenation unit (EDU) oxidizes isopropanol, forming acetone and hydrogen as the only detectable reaction products (Figure 2b).^[20] The two half-cell reactions are the anodic isopropanol oxidation reaction (IOR) and the cathodic hydrogen evolution reaction (HER).

The EC-LOHC acetone/isopropanol couple has a gravimetrical hydrogen capacity of 3.4 wt.% corresponding to 0.87 kWh $\rm L^{-1}$ (based on the hydrogen storage capacity, LHV $_{\rm H2}$ at 20 °C and 1 bar). Although this is lower than for the thermocatalytic LOHC systems, we show that the electrochemical advantageous accessibility of the acetone/isopropanol couple still has impressive potential for stationary energy storage applications.

The state-of-the-art research on the electrochemical hydrogenation of acetone to isopropanol is limited to just a few publications, some of which are relevant to this work.

Liang et al. and Bondue et al.[24-27] performed fundamental research at single-crystal electrodes investigating the ARR reaction mechanism and the catalyst's selectivity. Their results show a crystal-plane-dependent selectivity of the acetone reduction reaction. They observed a decreasing surface coverage with increasing overpotential and claimed competitive adsorption of acetone and hydrogen on the catalyst surface. Early works on the ARR in membrane electrode assemblies (MEA) were performed in a "thermally regenerative fuel cell design".[28-30] These studies aimed to use thermal energy for a thermal dehydrogenation of isopropanol and energy production through the exergonic ARR. Furthermore, they investigated the influence of acid addition to the electrolyte. The addition of acid leads to an improvement in cell performance. Whether this improvement was connected to the pre-protonation of acetone before adsorption, as Bondue et al.[27] mentioned, or solely an ionic conductivity-increase correlation, is unclear. Green et al.[31] already recognized the high prospects of the electrochemical hydrogenation of acetone, discovering high mass activity of the used platinum catalyst. They compared the reaction rates of an electrochemical system to a Parr reactor and showed a higher reaction rate per used catalyst for the electrochemical system than for the thermocatalytic one. Perry et al.[32] investigated the concept of a rechargeable liquid fuel cell with the acetone/isopropanol couple. The concept consisted of a hydrogenation reactor with acetone and hydrogen and a direct isopropanol fuel cell (DIFC) generating power. Generally, the parameters vary strongly among the electrochemical acetone hydrogenation MEA studies, ranging from pure acetone in the gaseous phase to a mixture of isopropanol, acetone, and sulfuric acid in water.[29-34]

The thermal LOHC terminology has inspired the term electrochemical dehydrogenation of isopropanol. [19] However, in the literature, electrochemical dehydrogenation is also known as electrochemical reforming or electrocoxidation of alcohols. [35,36] Despite its potential as EC-LOHC, the electrochemical dehydrogenation of isopropanol has been a somewhat overlooked system. In contrast, the electrochemical dehydrogenation of methanol and ethanol have drawn significant attention in recent years. [35-44] Considering the necessity of a CO₂-free energy infrastructure, the selective oxidation of isopropanol to acetone and hydrogen has a clear advantage over these primary alcohols, which form CO₂ as dehydrogenation product.

For the isopropanol oxidation reaction (IOR) on a bimetallic PtRu electrode, two separated oxidation peaks are the most distinctive feature. [20,21,45-47] The two peaks are roughly at 0.18 V versus the reversible hydrogen electrode (RHE) and 0.75 V versus RHE.[20] This two-peak phenomenon is also known for the DIFC with PtRu catalysts. [48-50] The DIFC shares the same anodic reaction, the IOR, but differs in its cathodic reaction (EDU: HER vs DIFC: Oxygen reduction reaction (ORR)). In the DIFC literature, this two-peak phenomenon has been correlated to an instability associated with a slow desorption of acetone from the catalyst surface. [45-49,51-53] Khanipour et al. [20] explained this behavior with different active catalyst sites. They showed that platinum exhibits only one IOR peak at 0.75 V versus RHE. Bimetallic PtRu, however, reveals an additional early IOR peak at 0.18 V versus RHE. They also confirmed by Electrochemical Real-Time Mass Spectrometry that the early IOR at PtRu forms no CO₂.[20,54] Mangoufis-Giasin et al.[21] confirmed this early oxidation peak on PtRu and demonstrated similar behavior for other longer secondary alcohols. They also showed that primary alcohols are oxidized to CO2, including C-C bond breakage at roughly 700 mV versus RHE and, therewith, preventing a reversible system design. The highly active and selective oxidation of isopropanol to acetone at low voltages (<0.35 V vs RHE) confirms the outstanding role of the acetone/isopropanol couple as an EC-LOHC. Consequently, the electrochemical dehydrogenation experiments in this study focused on the IOR on bimetallic PtRu at low voltages of <0.35 V versus RHE.

The scope of this work is to show the concept of a new hydrogen storage technology using the acetone/isopropanol EC-LOHC couple and to discuss how such a system could compete with state-of-the-art hydrogen storage technologies concerning energy efficiency (Figure 1). Based on the experimental results of the EC-LOHC system, this work compares different hydrogen storage technologies to the EC-LOHC, demonstrating the technical potential of the latter. Furthermore, we propose to use this EC-LOHC as a novel technology for stationary, seasonal, and off-grid energy storage applications.

2. Theoretical Background

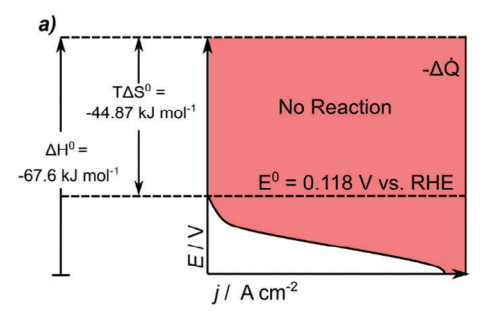
2.1. Thermodynamic Boundaries of the EHU and EDU

The thermodynamic correlations of the acetone hydrogenation and isopropanol dehydrogenation reactions are illustrated in **Figure 3**, whereby all thermodynamic data were retrieved from N.I.S.T.^[55–58] The ARR of the EHU (Figure 3a) is an exothermic and exergonic reaction in the herein investigated temperature ranges. The resulting fuel cell provides a standard reversible cell voltage (E^0_{rev}) of 0.118 V based on the Gibbs free energy and additional heat of -44.87 kJ mol $^{-1}$. Thus, for $E < E_{rev}$, the EHU is a galvanic- or fuel cell that can provide electric work and heat upon polarization. Accordingly, a galvanic cell should generate a voltage as high as possible at a given reaction rate.

The endothermic and endergonic IOR of the EDU (Figure 3b) needs heat and electric work of at least 44.87 kJ mol⁻¹ and 0.118 V at standard conditions. Thus, for $E > E_{rev}$, the resulting electrochemical system is an electrolytic or electrolysis cell producing hydrogen and acetone upon polarization. Accordingly,

16146840, 2025, 12, Downloaded from https://advanced.onlinelibrary.wiley.com/doi/10.1002/aemm.202403824 by Forschungszentrum Jülich GmbH Research Center, Wiley Online Library on [09/042025]. See the Terms and Conditions (https://onlinelibrary.

on Wiley Online Library for rules of use; OA articles are governed by the applicable Creative Commons L



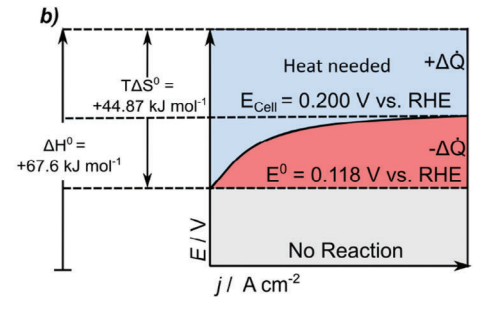


Figure 3. Relationship between voltage, enthalpy, Gibbs free energy, and consumed or produced heat during reaction for a) EHU and b) EDU. Due to the special form of the EDU, voltages above 0.2 V currents are decreasing again (see discussion of EDU cell process).

an electrolysis cell should maintain a voltage as low as possible at a given reaction rate.

That means the EHU and EDU are a reversible system sharing the identical E_{rev} . Altering the cell potential drives the reaction to the one or the other side. Therefore, the EHU and EDU can be operated in one electrochemical set-up, whereby the cell potential controls the direction of the reaction.

2.2. Integrating the EC-LOHC with Established Hydrogen Applications to Close a CO2 Emission-Free Power-To-Power Storage Cycle

The advantages of the electrochemical accessibility of the EC-LOHC are particularly evident for coupling the EHU/EDU to existing components of the hydrogen economy, e.g., water electrolysis and hydrogen fuel cells. The EHU produces electric energy and heat during hydrogenation, while the EDU consumes electric energy and heat during dehydrogenation. In contrast, existing thermal LOHC systems solely produce and consume heat upon hydrogenation and dehydrogenation. However, implementing electricity into a plant is more manageable than heat integration. For example, the electrical power generated by the EHU could lower the electricity cost of water electrolysis.

Furthermore, the EDU could be connected to a hydrogen fuel cell that consumes the produced hydrogen and provides electricity and exhaust heat for the EDU process. This integration concept seems worthwhile, considering a hydrogen fuel cell stack must be cooled during operation. ^[59] In fact, the exhaust heat of a hydrogen fuel cell (49 kJ $\text{mol}_{\text{H2}}^{-1}$) exceeds the heat necessary for the EDU (44.87 kJ mol^{-1}). Moreover, the waste heat of a commercial polymer exchange membrane fuel cell (PEMFC) is typically at \approx 80 °C, which is above the herein investigated EDU temperature range (30–70 °C) but distinctly lower than thermal LOHC dehydrogenation (>250 °C). ^[4,6,60]

Consequently, we see the technical potential of the EC-LOHC system to be best utilized in a power-to-power (PtP) cycle based on renewable energy, water electrolysis, EC-LOHC hydrogen storage, and hydrogen fuel cells. The freedom to couple a reversible EC-LOHC system with any existing water electrolysis or fuel cell technology could also shorten development time and reduce cost. Additionally, the hydrogen produced by the EDU could be coupled with industrial hydrogen applications, e.g., steel or chemical industries, to enable green heat provision and reduction processes (Figure 1).

2.3. Power-To-Power Efficiency Calculation

In order to fully evaluate the EC-LOHC in terms of its applicability, the experimental results must be seen in the context of existing hydrogen storage methods. Therefore, we calculated the PtP cycle efficiency and the specific storage efficiency for the different hydrogen storage systems, including the acetone/isopropanol hydrogen carrier. An ideal efficiency for the hydrogen storage process can be calculated to enable benchmarking of different storage technologies.

This ideal efficiency is the quotient of the work provided(w_{out}) / work needed(w_{in}) represented by a fuel cell (w_{FC}) and a water electrolyzer (w_{WF}):

$$\eta_{PtP, ideal} = \frac{\left| w_{out} \right|}{\left| w_{in} \right|} = \frac{\left| w_{FC} \right|}{\left| w_{WE} \right|} = \frac{21.66 \frac{kWh}{kg_{H_2}}}{51 \frac{kWh}{kg_{H_2}}} = 42.5 \% \tag{1}$$

For the calculation of $\eta_{PtP, ideal}$ the specific work of a PEMFC (21.66 kWh kg_{H2}⁻¹ at 65 % electrical fuel cell efficiency) and the specific work of a polymer electrolyte membrane water electrolysis (PEMWE) (51 kWh kg_{H2}⁻¹) were chosen.^[61,62] The storage efficiency ($\eta_{Storage}$) of each technology is calculated by comparing $\eta_{PtP, real}$ to $\eta_{PtP, ideal}$:

$$\eta_{Storage} = \frac{\eta_{PtP, real}}{\eta_{PtP, ideal}} \tag{2}$$

This real efficiency is calculated by inserting a hydrogen storage system, whereby CH_2 and LH_2 increase w_{in} . In contrast, for LOHC and the acetone/isopropanol EC-LOHC, the hydrogenation of LOHC- and EC-LOHC- are exergonic reactions and, thus, can generate work. Therefore, the general term comprising all hydrogen storage technologies can be given as:

$$\eta_{PtP, real} = \frac{\left| w_{out} \right|}{\left| w_{in} \right|} = \frac{\left| w_{FC} - w_{release \ H_2} \right|}{\left| w_{WE} + w_{storage \ H_2} \right|}$$
(3)

where $w_{storage\ H_2}$ is the work provided by LOHC- or EC-LOHC-hydrogenation or the work needed for CH₂ and LH₂ storage. $w_{release\ H_2}$, on the other hand, is the work needed by LOHC+ or EC-LOHC+ dehydrogenation. For CH₂ and LH₂, this value is zero.



www.advenergymat.de

For thermocatalytic LOHC+ dehydrogenation, a share of hydrogen has to be burned to provide heat for the endothermic dehydrogenation reaction.^[4,63]

Accordingly, the energetic cost for H_xBT or H_xDBT dehydrogenation is paid based on the LHV_{H2} and does not have to be paid by the fuel cell's electrical work: [64]

$$\frac{LHV_{H_2} - 11.82 \frac{kWh}{kg_{H_2}}}{LHV_{H_3}} = 64.6 \%$$
 (4))

This means a share of 35.4 % of the hydrogen produced by water electrolysis must be burned to provide heat for H_xBT or H_vDBT dehydrogenation.^[65]

At 100% thermal efficiency of hydrogen combustion for LOHC+ dehydrogenation, $|w_{out, H_xBT \text{ or } H_xDBT}|$ can therefore be calculated by:

$$w_{out, H_xBT \text{ or } H_xDBT} = w_{FC} - w_{release H_2}$$

$$= LHV_{H_2} \cdot \eta_{FC} \frac{LHV_{H_2} - 11.82 \frac{kWh}{kg_{H_2}}}{LHV_{H_1}}$$

$$= w_{FC} - (\eta_{FC} \cdot 11.82 \frac{kWh}{kg_{H_2}})$$
 (5)

For the EC-LOHC, the specific work produced (EHU) or required (EDU), respectively, can be calculated as:

$$w_{\text{storage } H_2 \text{ (EHU)}| \text{ release } H_2(EDU)} = \frac{\pm Q \cdot |E|}{m_{H_2}} = \frac{\pm |E| \cdot F \cdot z_{H_2}}{M_{H_2}}$$
(6)

where $w_{storage\ H_2\ (EHU)|\ release\ H_2(EDU)}$ is the specific electrical work provided/needed per kg of hydrogen given as $kWh\ kg_{H_2}^{-1}$. Q and E are the charge and the operational voltage during the EHU/EDU, respectively. Using Faraday's law, the specific work provided/needed can be calculated using the Faraday constant F (96 485 C mol⁻¹), the electrochemical equivalent number (z_{H_2} = 2) and the molar mass of hydrogen M_{H_2} .

The work is defined with a negative sign for the EHU (work provided) and a positive sign for the EDU (work needed). By this means, we correlate the current as our targeted reaction rate ($I_{measured} = I_{H_2}$), assuming a Faradaic efficiency of 100 %. In contrast to the early selective IOR at PtRu, there are still no comprehensive studies of the ARR that quantify liquid and gaseous products. [20,21,45] Therefore, the Faradaic efficiency for the EHU and EDU is a favorable assumption.

Representative and detailed $\eta_{PtP, real}$ and $\eta_{Storage}$ calculations with the corresponding formula and numerical values for each of the storage technologies are given in Section S3 (Supporting Information).

In principle, the detour via the PEMFC and PEMWE reference is not necessary to evaluate a storage technology efficiency. However, in a PtP chain consisting of thermally and electrically coupled water electrolysis and fuel cell systems (WE/EHU and EDU/FC), it is required to be considered. For the EC-LOHC system, we simplified the efficiency calculation by only considering the electric work because the exhaust heat of a coupled fuel

cell exceeds the necessary heat for the EDU. Implicitly, we assumed a perfect heat integration. The provided exhaust heat of the exergonic EHU system is likewise neglected in this work. Within these premises, the low-temperature (<80 °C) EC-LOHC system particularly benefits from the coupling compared to the other hydrogen storage systems. Neither a thermocatalytic LOHC (>250 °C), CH $_{\rm 2}$, nor LH $_{\rm 2}$ could utilize the PEMFC exhaust heat to a similar extent. Nevertheless, we feel this is a legitimate comparison for a PtP case revealing the advantages of this EC-LOHC system.

Due to complicated comparability, time-dependent storage losses such as the so-called LH $_2$ "boil-off" are not considered. The efficiency data for LH $_2$ storage must be regarded as best-case assumptions that neglect any boil-off losses. No relevant storage losses are expected for the aqueous ≤ 2 M acetone/isopropanol solutions, as the boiling points of both 2 M acetone and 2 M isopropanol are above 80 °C. $^{[67-69]}$ Therefore, the ACE/IPA system is considered liquid during operation (30–70 °C) and storage.

2.4. Stable Hydrogen Reference Potential for the Dehydrogenation

The E^0 of the HOR/HER (Figure 2) at pH 0 is 0 V. However, this is only valid for standard conditions, including a hydrogen partial pressure of unity. Therefore, a stable hydrogen partial pressure is mandatory for a stable hydrogen electrode potential to investigate the reaction rate-determining ARR or IOR. However, during the EDU operation, at low current densities and without an active hydrogen supply, the cathodic HER would be insufficient to generate a steady cathodic hydrogen partial pressure.^[70] Consequently, the cathodic potential would shift during operation, making the experimental polarization curves meaningless. This problem can be solved by constantly flushing the cathode with hydrogen, ensuring a stable cathode potential. To minimize the possible impact of hydrogen crossover, we refrained from using a pure hydrogen supply for the EDU but instead fed a diluted 5 vol% H₂ reforming gas.^[70] This causes a Nernstian shift of the cathodic potential:

$$E_{EDU, cathode} = E^{0} + \frac{RT}{zF} \ln \frac{a(ox)}{a(red)} = 0 V + \frac{RT}{zF} \ln \frac{1}{p_{H_{2}}}$$
(7)

 E^0 is the standard potential for the HER, R is the gas constant (8.314 J molK⁻¹), T is the temperature in Kelvin, and p_{H_2} is the partial pressure of hydrogen.

Because the HER increases the p_{H_2} during the experiment, the 5 vol% H_2 flow rate was chosen to be as high as 1 L min $^{-1}$ to limit the maximum potential offset caused by the HER to $\Delta 6$ mV according to the obtained current densities. Consequently, the cathode potential can be considered a stable reference electrode during the open circuit voltage (OCV) and electrochemical dehydrogenation (detailed calculations are in the Section S4, Supporting Information).

For an easier comparison of the EDU to the EHU, the potential in the following EDU graphs is corrected by this Nernstian shift ($E_{EDU,\;cathode}$: 40 mV at 30 °C, 41 mV at 40 °C, 44 mV at 50 °C, 46 mV at 60 °C, 50 mV at 70 °C) and given as E_{calc} for calculated potential based on Equation (7) (experimental 5 vol% H_2

16146840, 2025, 12, Downloaded from https://advanced.onlinelibrary.wiley.com/doi/10.1002/aenm.202403824 by Forschung

zentrum Jülich GmbH Research Center, Wiley Online Library on [09/04/2025]. See the Terms

conditions) on Wiley Online Library for rules of use; OA articles are governed by the applicable Creative Commons L



data in Figures S8–S11, Supporting Information). So far in the literature, dry or water-flushed cathodes have been investigated for methanol and ethanol electrochemical dehydrogenation. [71–74]

3. Results and Discussion

3.1. Technical Feasibility of Separated ACE Hydrogenation and IPA Dehydrogenation in Electrochemical Cells

The results of the separated EHU and EDU experiments are discussed in the following section. Both cells share an electrode at which the organic compound reaction takes place and an electrode at which the hydrogen reaction takes place (Figure 2).

The HOR and the HER at platinum are among the fastest-known electrochemical reactions in acidic environments.^[75,76] Thus, the required overpotentials to drive these reactions are negligibly small. Therefore, the EHU (cell) is limited by the ARR (reaction), whereas the IOR (reaction) limits the EDU (cell).

All experiments used the same cell fixture configuration and materials to support the concept of a reversible system, except for the metal loading of the ARR/IOR side. 2 $\rm mg_{PtRu}$ cm $^{-2}$ was chosen for the endergonic EDU experiments, whereas 1 $\rm mg_{PtRu}$ cm $^{-2}$ was sufficient for the exergonic EHU experiments. This was done to achieve similar current densities for both setups. Despite this slight difference, the system's similarity supports the option of having a future hydrogenation and dehydrogenation system within one stack. Because the investigated parameters impact the EHU and EDU similarly and often have the same explanations, the following section is divided into the three examined parameter sets and explains how they affect the EHU and EDU.

3.2. Temperature Variation

Figure 4 depicts the influence of varying temperatures on the EHU and EDU of a 1 M feed solution. The EHU polarization curves (Figure 4a) show a low current density region with a steep potential drop, a middle current density region with a flattened potential drop, and a fast voltage drop region around the peak current density. These characteristics could be similar to an activation, an ohmic, and a mass transport limiting region, which are typical for fuel cells.^[1] However, the characteristics of established fuel cell systems are more distinct and have already been examined in more detail. An exact determination or evaluation of the different regions of the ARR has not been performed in literature.

The shape of the EDU polarization curves (Figure 4b) is dominated by the early isopropanol oxidation peak at PtRu.^[20,21] Voltages higher than this oxidation peak lead to lower current densities, which cause unfavorable higher electric costs for dehydrogenation.

Rising temperatures are expected to cause lower E_{rev} , improved reaction kinetics, and increased ionic conductivity for both galvanic and electrolysis cells.^[1,77] In fact, the onset potential (potential at 1 mA cm⁻²) for both systems decreases as the temperature rises. While the onset potentials of the EHU drop by 20 mV from 135 mV at 30 °C to 115 mV at 70 °C, the onset potentials of the

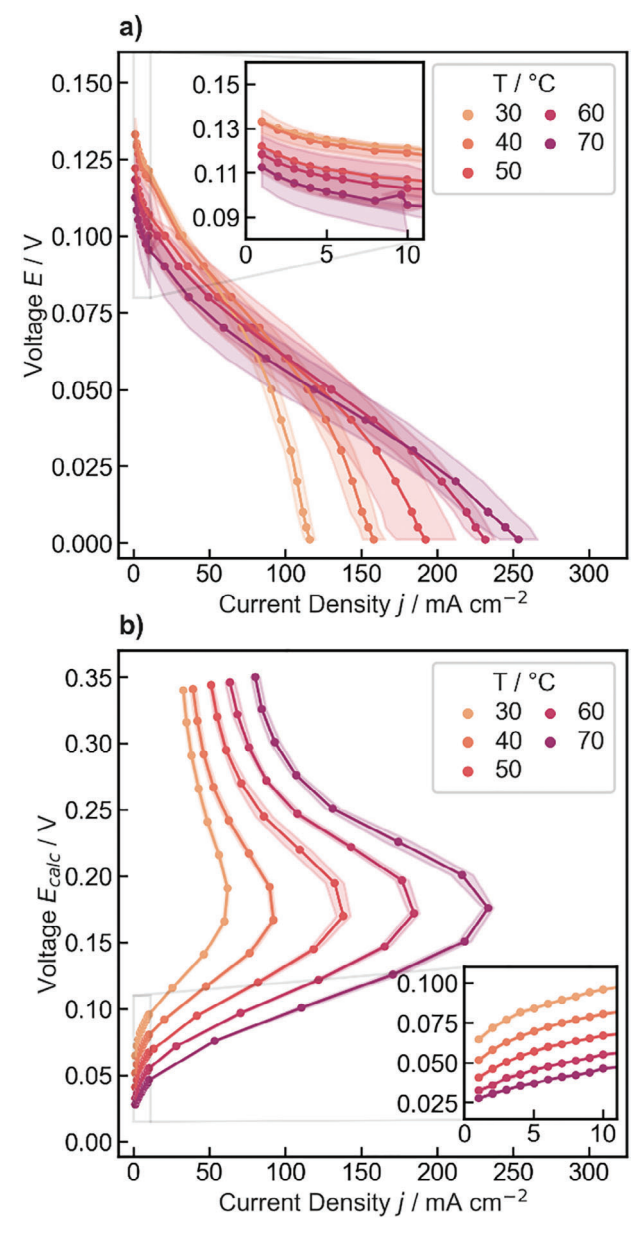


Figure 4. Polarization curves at varying temperatures of a) EHU for 1 M acetone and b) EDU for 1 M isopropanol. For an easier comparison of the data, the voltage of b) is corrected by the Nernstian shift caused by the 5 % $\rm H_2$ feed according to Equation (7). The uncorrected experimental data of b) is given in the supporting information Figure S7 (Supporting Information). The shaded lines represent the standard deviation of three independently measured MEAs.

EDU drop by 37 mV from 65 mV at 30 °C to 28 mV at 70 °C. This different temperature-dependent voltage drop could stem from different hydrogen crossover rates ($\rm H_2$ crossover data given in Figure S2, Supporting Information). While the EHU is provided with humidified hydrogen, the EDU counter electrode is fed by humidified reforming gas (5 vol% $\rm H_2$). Furthermore, acetone and isopropanol can cause distinct and different ionomer swelling, causing different crossover rates. This mechanism is

6146840, 2025, 12, Downloaded from https://advanced.onlinelibrary.wiley.com/doi/10.1002/aenm.202403824 by Forschungs

zentrum Jülich GmbH Research Center, Wiley Online Library on [09/04/2025]. See the Terms

conditions) on Wiley Online Library for rules of use; OA articles are governed by the applicable Creative Commons

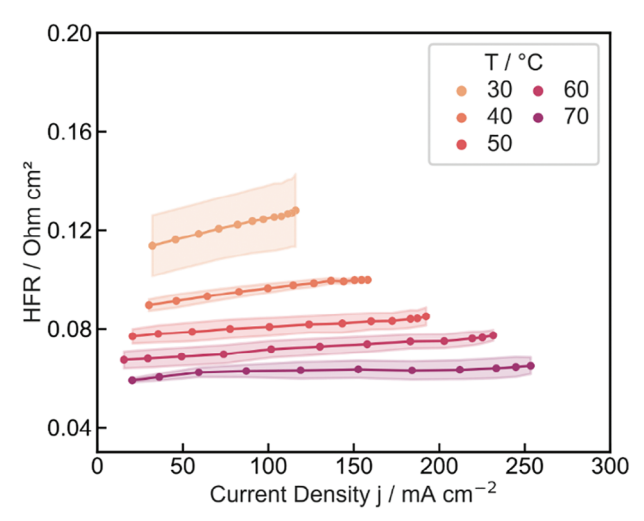


Figure 5. HFR of the EHU at varying temperatures for 1 M acetone. The EIS spectra were recorded potentiostatically. Nevertheless, the polarization curves are depicted with the current density on the X-axis due to convention. The current density represents the average system response for the potentiostatic measurement, whereby the current density error bars are omitted for clarity (EHU & EDU experimental data with current density error bars are given in Figures S4 and S7, Supporting Information). The shaded lines represent the standard deviation of three independently measured MEAs.

well-known from direct alcohol fuel cell (DAFC) systems and can be considered likely. $^{[78]}$

Higher temperatures also lead to faster reaction kinetics and rapid reactant diffusion. The peak current density of the EHU doubles between 30 °C and 70 °C, from 116 to 253 mA cm $^{-2}$, while the peak current density of the EDU almost quadruples from 62 to 233 mA cm $^{-2}$. The endergonic IOR particularly benefits from rising temperatures, which explains the pronounced peak current density increase for the EDU system. Nonetheless, it becomes evident that the IOR is the more arduous reaction, especially when taking into account the different electrocatalyst loadings for these experiments (ARR: 1 mg $_{\rm PtRu}$ cm $^{-2}$, IOR: 2 mg $_{\rm PtRu}$ cm $^{-2}$). This discrepancy could be attributed to a slow desorption of acetone from the PtRu catalyst, which is also indicated for the direct isopropanol fuel cell at PtRu electrodes. $^{[45,46,49,51]}$

One additional reason for improved performance at elevated temperatures is that the conductivity of the ionomer massively benefits from an increase in temperature, as seen in the EHU high-frequency resistance (HFR) data (Figure 5). The HFR trends apply to the EHU and EDU to the same extent and, therefore, are depicted as an example (EDU HFR data are portrayed in Figures S8–S10, Supporting Information). Considering the high impact of rising temperatures on the achieved reaction rates makes the temperature a crucial parameter for designing an EHU/EDU system.

3.3. Reactant Concentration Variation

Figure 6 depicts the influence of varying feed concentrations at $50~^{\circ}\text{C}$ of acetone on the EHU and isopropanol on the EDU. At $50~^{\circ}\text{C}$, the EHU and EDU exhibit considerable reaction rates

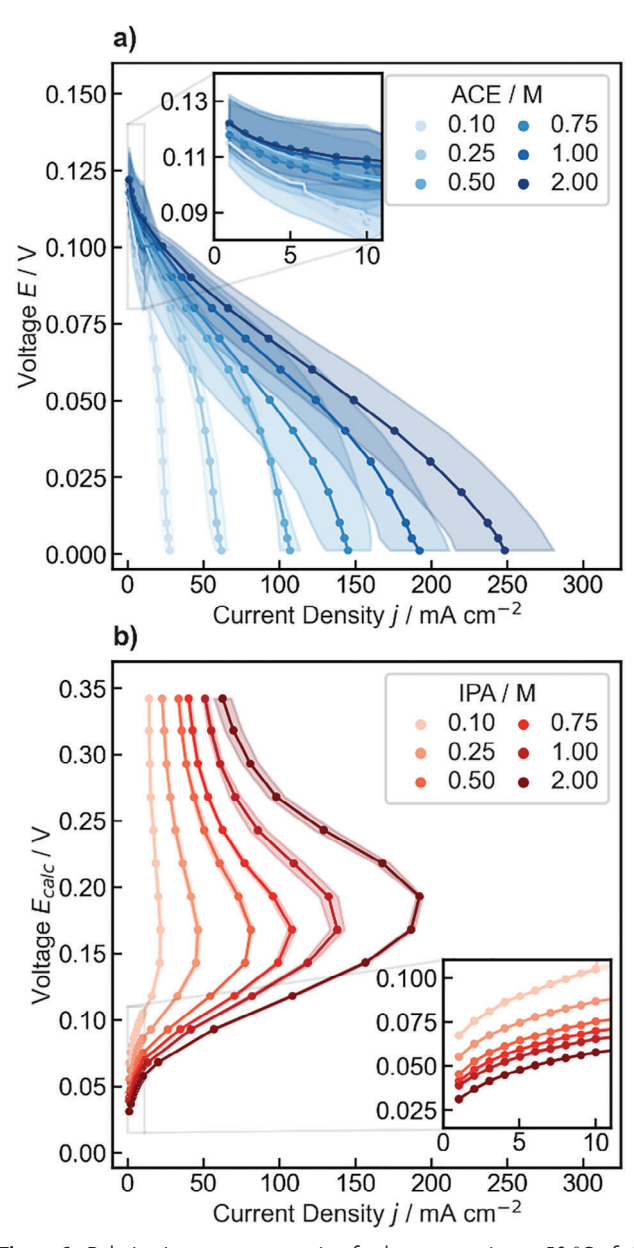


Figure 6. Polarization curves at varying feed concentration at 50 °C of a) EHU and b) EDU. For an easier comparison of the data, the voltage of b) is corrected by the Nernstian shift caused by the 5 % $\rm H_2$ feed according to (7). The uncorrected experimental data of b) is given in Figure S8 (Supporting Information). The shaded lines represent the standard deviation of three independently measured MEAs.

and low HFRs, so the influence of concentration is clearly distinguishable. Furthermore, 50 $^{\circ}\text{C}$ is a practically relevant temperature considering a coupling to low-temperature WE and FC.

As for DAFC systems, we fed diluted aqueous acetone/ isopropanol solutions to mitigate fuel crossover, in order to mitigate unfavorable mixed potentials. [65] Moreover, the proton exchange electrolytes require water to ensure sufficient ionic conductivity. [79] Further information on the hydrogen capacity of the aqueous solutions is given in Section S10 (Supporting Information).

ENERGY MATERIALS

www.advenergymat.de

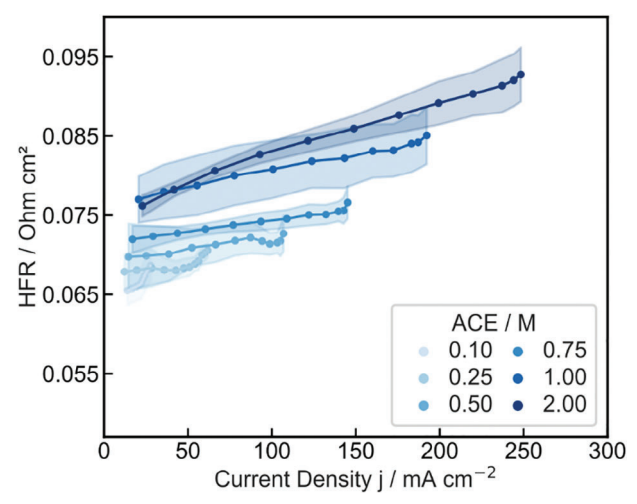


Figure 7. HFR of the EHU for varying acetone concentrations at 50 $^{\circ}$ C. The EIS spectra were recorded potentiostatically. Nevertheless, the polarization curves are depicted with the current density on the X-axis due to convention. The current density represents the average system response for the potentiostatic measurement, whereby the current density error bars are omitted for clarity (EHU & EDU experimental data with current density error bars are given in Figures S5 and S8, Supporting Information). The shaded lines represent the standard deviation of three independently measured MEAs.

According to the Nernst equation, E_{rev} increases with increasing activity of the oxidized species (acetone), whereas E_{rev} decreases with increasing activity of the reduced species (isopropanol). Although it is impossible to calculate a theoretical E_{rev} without both species present, the trends can be observed: While the onset potential of the EHU increases with increasing acetone concentration from 117 mV at 0.1 m ACE to 124 mV at 2 M ACE, the onset potential of the EDU decreases with increasing isopropanol concentration from 69 mV at 0.1 m IPA to 33 mV at 2 m IPA.

Presumably, different fuel crossover rates caused by distinct acetone or isopropanol membrane swelling and different hydrogen feeds can explain the different changes in onset potentials between EHU and EDU. The peak current density of the EHU rises from 28 mA cm $^{-2}$ at 0.1 m ACE to 250 mA cm $^{-2}$ at 2 m ACE. Furthermore, the corresponding maximum power density of 7.4 mW cm $^{-2}$ for the 2 m ACE solution is the highest reported power density for an acetone hydrogenation cell (Figure S6, Supporting Information).

The peak current density of the EDU rises from 22 mA cm $^{-2}$ at 0.1 M IPA to 192 mA cm $^{-2}$ at 2 M IPA. The increasing current densities could be explained by an increased reactant catalyst surface coverage, faster desorption, and enhanced mass transport.

On the other hand, higher organic concentrations slightly increase the membrane resistance (HFR) (**Figure 7**), possibly through the decrease of water fraction inside the membrane, thus decreasing the proton conductivity inside the membrane.^[18] Similar findings have been shown by Perry et al.^[32] for the DIFC. The current densities obtained for both directions of the EC-LOHC with a 2 M solution at 50 °C are similar to those of commercial alkaline water electrolyzers.^[80,81] Although this system is differ-

ent, it shows that the current densities for this non-optimized electrochemical concept are already of relevant magnitude.

3.4. Mixed Acetone and Isopropanol Solution Variation

In applied systems, as the EC-LOHC system continuously produces acetone or isopropanol, the EHU/EDU will not be operated with pure solutions but with mixed acetone/isopropanol solutions. Therefore, a mixed feed variation with a total of 2 M organic solution at 50 °C was conducted (**Figure 8**).

As the oxidized species (acetone) and the reduced species (isopropanol) are both present in low molarity, E_{rev} can be calculated according to the Nernst equation. Subsequently, the OCV is compared to the theoretical E_{rev} in Figure 8d. The OCV observed for the different solutions decreases with increasing isopropanol concentrations, following the thermodynamically predicted trend yet revealing a slight offset to lower voltages. The OCV reflects E_{rev} impaired by internal currents caused by fuel crossover, fuel impurities, and catalyst surface oxides. [82,83] Furthermore, neither platinum nor ruthenium oxidation is thermodynamically expected within the examined voltage range. [84]

For cell operation, the EHU/EDU can be driven by applying a corresponding overpotential to the ACE/IPA-dependent E_{rev} . Hence, the EC-LOHC-/EC-LOHC+ reaction equilibrium limits the possible overpotential at a given absolute potential. (The overpotential $\eta=E-E_{rev}$ is the potential that must be paid to drive a reaction at a given reaction rate.) This results in decreasing current densities at increasing isopropanol concentrations for the EHU, whereas increasing current densities at increasing isopropanol concentrations for the EDU (Figure 8a,b). For the thermocatalytic LOHC terminology, this LOHC-/LOHC+ reaction equilibrium is also described as the degree of hydrogenation (DoH) and given in percent. [85] Shifting the reaction equilibrium to the product direction can also promote mass transport limitations due to lower fuel availability and partial product surface coverage of the catalyst.

The peak current densities of the EHU are less dependent on the DoH than the EDU. For example, the pure 0.1 M ACE solution has a peak current density of 28 mA cm⁻², whereas the 0.1 M ACE|1.9 M IPA solution has a peak current density of 17 mA cm⁻² (Figures 6a and 8a) for the EHU. In contrast, the pure 1 M IPA solution has a peak current density of 138 mA cm⁻², whereas the 1 M ACE|1 M IPA solution has a peak current density of only 39 mA cm⁻² (Figures 6b and 8b) for the EDU. Nevertheless, substantial dehydrogenation reaction rates were obtained at 0.15 V for a 1:1 ratio of ACE/IPA, representing a DoH of 50 %. The different dependency of the EHU/EDU on the DoH allows the assumption that the EHU can achieve an almost complete conversion to isopropanol. At the same time, the EDU may only be operated up to 50 % DoH. In this case, higher system efficiency can be achieved at the expense of hydrogen storage capacity.

The results so far have shown that the EDU is the limiting process of the EC-LOHC concept. Overall, the corresponding reaction rates are lower than for the EHU and are hampered to a greater extent by a product-shifted EC-LOHC-/EC-LOHC+ reaction equilibrium. The likely reason for this observation is the slow desorption of acetone from the PtRu catalyst. [45,46,49,51]

16146840, 2025, 12, Downloaded from https://advanced.onlinelibrary.wiley.com/doi/10.1002/aenm.202403824 by Forschungs

szentrum Jülich GmbH Research Center, Wiley Online Library on [09/04/2025]. See the Terms and Conditions (https://onlinelibrary.wiley.

conditions) on Wiley Online Library for rules of use; OA articles are governed by the applicable Creative Commons L

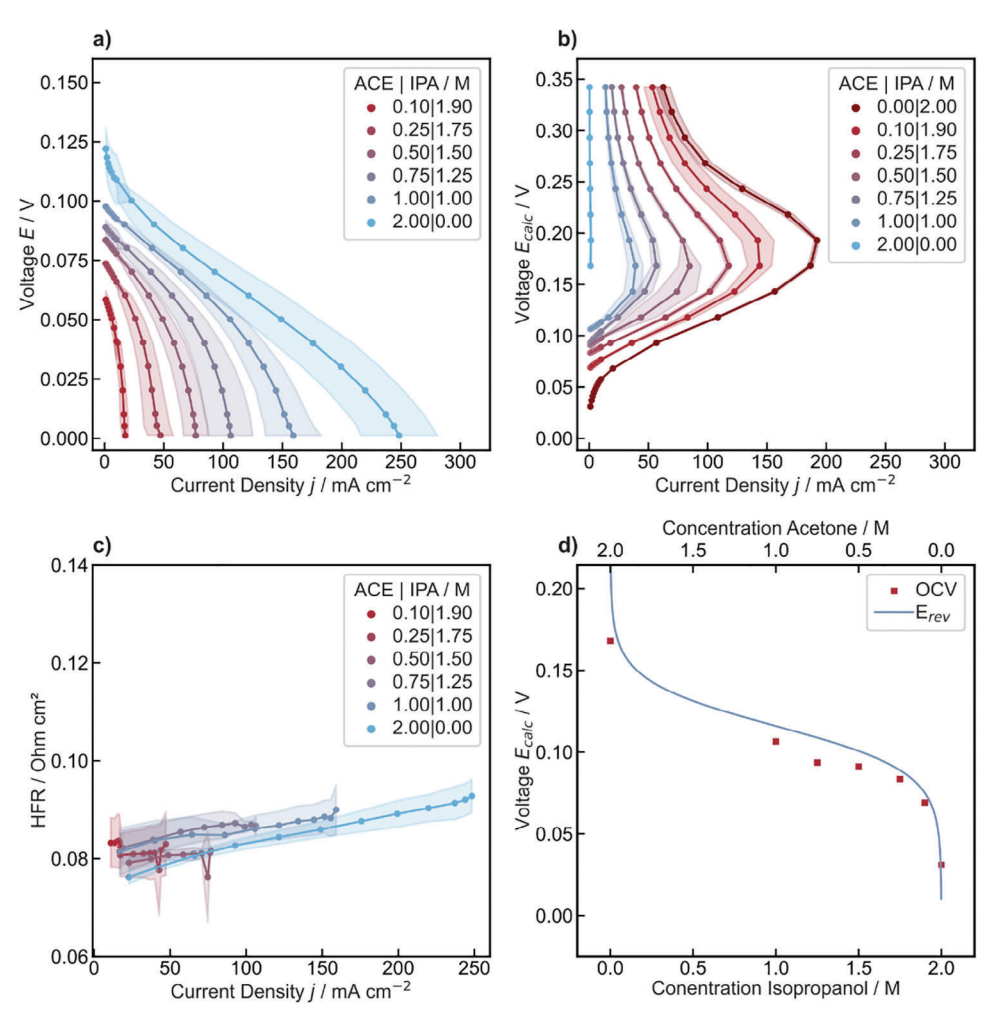


Figure 8. Polarization curves at varying acetone/isopropanol rations with a total organic concentration of 2 M at 50 °C of a) EHU and b) EDU. For an easier comparison of the data, the voltage of b) is corrected by the Nernstian shift caused by the 5 % H_2 feed according to (7). The uncorrected experimental data of b) is given in Figure S9 (Supporting Information). c) HFR of the EHU for varying acetone/isopropanol rations with a total organic molarity of two at 50 °C. The EIS spectra were recorded potentiostatically. Nevertheless, the polarization curves are depicted with the current density on the X-axis due to convention. The current density represents the average system response for the potentiostatic measurement, whereby the current density error bars are omitted for clarity. (EHU & EDU experimental HFR data with current density error bars are given in Figures S6 and S9, Supporting Information). The shaded lines represent the standard deviation of three independently measured MEAs. d) OCV versus E_{rev} for the measured acetone/isopropanol ratios.

To demonstrate the prospects of the EDU, temperature, isopropanol concentration, and an increased flow rate were put to optimum conditions, achieving up to 375 mA cm⁻² at 0.19 V (Figure S11, Supporting Information). The EDU optimization can be seen as a relevant outlook on how the EDU can be further optimized, as given in Section S9 (Supporting Information).

Applying a potential between OCV and 342 mV in the EDU set-up for a 2 M ACE solution without isopropanol results in a peak current density of 1.21 mA cm⁻², indicating no further oxidation of acetone in the studied potential range.^[20] The negligible current densities probably result from the membrane's lack of a perfect electrical insulator and hydrogen crossover. The concept of the acetone/isopropanol EC-LOHC couple crucially depends upon the reversibility of the hydrogenation and dehydrogenation. Therefore, no further oxidation of acetone within the investigated potential range is essential to the EC-LOHC concept.

Figure 8c displays no considerable differences between the different ACE/IPA ratios on the proton conductivity inside the membrane. Hence, the amount of acetone and isopropanol is more relevant to the HFR than their ratio.

3.5. Energy Efficiencies for the ACE/IPA Electrochemical LOHC Cycle

The following section compares the ACE/IPA EC-LOHC results to other hydrogen storage technologies in the context of a PtP chain. The different options for hydrogen storage vary considerably in their respective storage efficiencies and conceptual advantages:

Hydrogen compression to 700 bar corresponds to an energy cost of 5 kWh kg $_{\rm H2}^{-1}$, resulting in a volumetric energy density of 1.27 kWh L $_{\rm H2}^{-1}$ (based on LHV $_{\rm H2}$ at ambient temperature). [86,87]



www.advenergymat.de

Table 1. Efficiencies of different hydrogen storage technologies in a PtP chain elucidated by the calculations based on Equation (3) and (4). $\eta_{Storage}$ is calculated inserting η_{PtP} in Equation (2). H_x -BT or H_x -DBT efficiencies are given without (w/o) heat integration. The EHU / EDU voltages for this depiction are chosen based on the experimental results of this work. The red and blue star correspond to the markers in Figure 9.

Storage technology	$w_{Release, H_2}$ [kWh kg _{H2} ⁻¹]	$w_{Storage, H_2}$ [kWh kg _{H2} ⁻¹]	η _{PtP} [%]	η _{Storage} [%]	Refs.
CH ₂ @ 350 bar	0	4.03	39.4	92.7	[86]
CH ₂ @ 700 bar	0	5	38.7	91.1	[86]
LH ₂ @ 20 K, 1 bar	0	10	35.5	83.5	[⁹⁰ , ⁹¹]
Thermocatalytic LOHC w/o heat integration $(H_x$ -BT or H_x -DBT)	11.82	0	27.4	64.5	[4,63]
EC-LOHC: EHU @ 0.075 V, EDU @ 0.075 V ★	2.01	-2.01	40.1	94.4	This work
EC-LOHC: EHU @ 0.00 V, EDU @ 0.15 V ☆	4.02	0	34.6	81.4	This work

This value lies between the two boundaries of isothermal and adiabatic hydrogen compression and represents a technically realistic value. CH2 is the most mature hydrogen storage technology but requires expensive storage tanks.[88,89] The energetic costs for hydrogen liquefication are at 10 kWh kg_{H2}⁻¹, resulting in a volumetric energy density of 2.34 kWh $L_{\rm H2}^{-1}$ (based on LHV_{H2} at -253 °C and 1 bar). [90-92] This value is derived from a state-of-the-art five-ton-per-day hydrogen liquefier with liquid nitrogen precooling.^[90] Due to the lack of cooling during transport, the LH₂ storage efficiency gets further reduced significantly by hydrogen evaporation, the so-called "boil-off". [2,66] For thermocatalytic LOHC-based storage processes, a share of hydrogen has to be burned to provide heat for the endothermic dehydrogenation reaction if heat integration with the energetic utilization of the released hydrogen or an external heat source is not possible.[4,63] According to the literature, the dehydrogenation for benzyl toluene (H₀-BT) / perhydro-benzyl toluene (H₁₂-BT) and dibenzyl toluene (H₀-DBT) / perhydro-dibenzyl toluene (H₁₈-DBT), result in energetic cost of 11.8 kWh ${\rm kg_{H2}}^{-1}$ reaching hydrogen capacities of 6.2 wt% and volumetric energy densities of 1.85 kWh L^{-1} (H₁₂-BT) and 1.91 kWh L^{-1} (H₁₈-DBT), respectively (based on the hydrogen storage capacity, LHV $_{\rm H2}$ at 20 °C and 1 bar).[4,63,93]

The corresponding PtP efficiencies for these different hydrogen storage technologies, including the EC-LOHC, are calculated using Equations (3), (5), and (6). Subsequently, η_{PtP} is inserted into Equation (2) to calculate $\eta_{Storage}$. The efficiencies of the corresponding hydrogen storage technologies are summarized in Table 1.

State-of-the-art compressed hydrogen technologies show storage efficiencies of 92.7 % (350 bar) and 91.1 % (700 bar), outperforming most other technologies. LH $_2$ can achieve storage efficiencies of 83.5 % when neglecting time-dependent "boil-off" [2.66] losses. EC-LOHC (94.4 % when EHU @0.075 V, EDU @0.075 V, 81.4 % when EHU @0.00 V, EDU @0.15 V) exceeds thermocatalytic LOHCs (64.5 %) significantly and performs slightly better than CH $_2$ if the EDU can function at low voltages. This comparison to thermocatalytic LOHC sets out the benefits of a low-temperature EC-LOHC system in numbers.

The main reasons for the high EC-LOHC efficiency are a) the possibility of a heat integration with a PEMFC due to the low-temperature operation of the EDU ($T_{\rm operation}=30$ –

70 °C) in comparison to current thermochemical LOHC systems ($T_{\rm operation} = 250-300$ °C), b) the low energy costs for hydrogen release in the EDU step, and c) the electric energy generation during EHU operation.

One noticeable difference between the EC-LOHC, CH2, and LH₂ is shown in Figure 9. As the experimental results section explains, shifting EC-LOHC- and EC-LOHC+ ratios leads to a Nernst shift that causes varying storage efficiencies: The higher the DoH (isopropanol concentration), the lower the potential provided by hydrogenating acetone. In contrast, the higher the DoH, the lower the potential needed to dehydrogenate isopropanol, leading to decreased efficiency throughout dehydrogenation/hydrogen release. For the EHU, the upper and lower voltage limits are set to 0.075 V and 0 V, respectively. This is a range where the EHU generates electric energy. For the EDU, voltages between 0.075 V and 0.15 V are considered. This range enables the reversible isopropanol oxidation to acetone for the PtRu catalyst employed in this study.[21] It is important to note that a DoH of 50 % can be achieved when running the system between these voltages.

Due to the high energy costs of water electrolysis (51 kWh kg^{-1}_{H2}),[61,62] the impact of the EHU on cost reduction is relatively small. For example, at 0.075 V, the EHU produces 2.01 kWh kg⁻¹_{H2}, which leads to a 3.9 % cost reduction when directly coupling water electrolysis and EHU. On the other hand, the EDU considerably reduces the power yield of a PEMFC $(21.66 \text{ kWh kg}^{-1}_{H2})$, [61,62] e.g., at 0.075 V, the EDU consumes 2.01 kWh kg^{-1}_{H2} , which correlates to a reduction of 9.3 %. It can be deduced that the EDU influences PtP efficiency more than the EHU. This result is also depicted in Figure 9, where the EC-LOHC efficiency varies to a greater extent when varying the EDU voltage (Figure 9b) compared to the EHU voltage variation (Figure 9a). Accordingly, the EDU should be operated at the lowest possible voltages to achieve the highest possible PtP efficiency. On the other hand, the EHU can also be operated at low voltages associated with low electricity generation, as the EHU only makes a minor efficiency contribution. As low EHU voltages are related to high current densities / high reaction rates, such operation points can be meaningful to store hydrogen at high rates.

Overall, it becomes apparent that the EC-LOHC concept can compete with the more established hydrogen storage systems in

16146840, 2025, 12, Downloaded from https://advanced.onlinelibrary.wiley.com/doi/10.1002/aenm.202403824 by Forschung

zentrum Jülich GmbH Research Center, Wiley Online Library on [09/04/2025]. See the Terms and Conditions (https://onlinelibrary.wiley

conditions) on Wiley Online Library for rules of use; OA articles are governed by the applicable Creative Commons

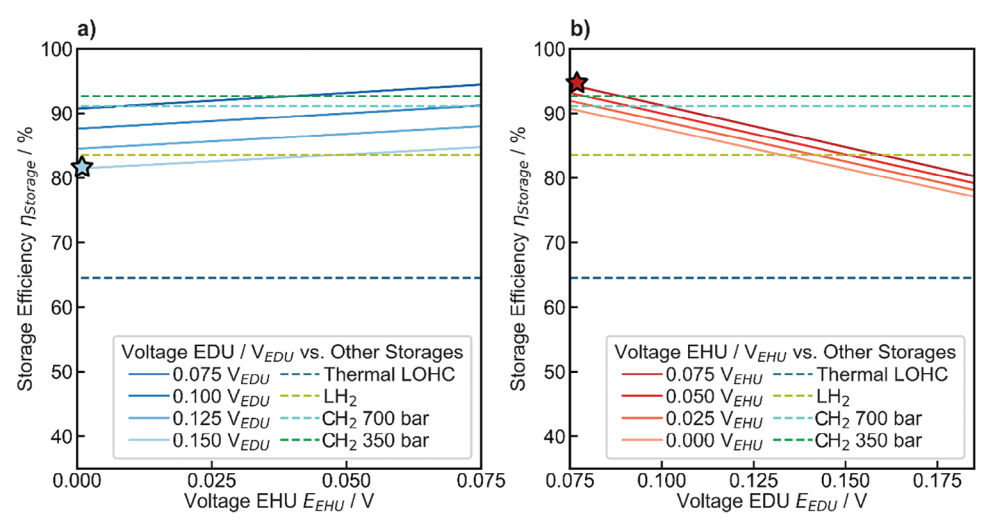


Figure 9. Graphical efficiency classification of the EC-LOHC to CH_2 , LH_2 and thermal LOHCs (H_x -BT or H_x -DBT) for a) four fixed EDU operation voltages and b) four fixed EHU operation voltages. The slope of the EC-LOHC represents the shifting EC-LOHC-/EC-LOHC+ reaction equilibrium (DoH). Dashed lines represent voltage-independent storage efficiencies of CH_2 , LH_2 and thermal LOHCs. The blue star marker in a) represents entry 6 of Table 1 (EHU @ 0.00 V, EDU @ 0.15 V). The red star marker represents entry 5 of Table 1 (EHU @ 0.075 V, EDU @ 0.075 V).

a PtP cycle, making it a potential candidate for a new class of stationary, long-term hydrogen storage.

In particular, the comparison with thermocatalytic LOHC systems shows that the EC-LOHC concept can have considerably higher efficiencies while still having the advantage of cheap liquid fuel storage. Yet the volumetric storage capacity is lower than that of thermocatalytic LOHC systems due to the lower hydrogen capacity of the acetone/isopropanol and the need to operate this EC-LOHC in the form of aqueous solutions.

3.6. Material-Related Challenges and Outlook

Our experimental results are a fair representation of the EHU and EDU within an overall testing time of several hours. However, the results do not represent the system in long-term operation. Degradation effects would have to be investigated in depth to make statements about long-term stability; for example, degradation was investigated for many decades for PEMFC. Thus, long-term degradation is beyond the scope of this concept study. Nevertheless, we can use our data as a function of time to identify material-related challenges and provide possible solutions.

Figure 10 depicts representative EHU and EDU raw data of a 2 min hold as a function of time and a corresponding decay rate between 31–120 s. The chosen potentiostatic holding points of 1 and 90 mV for the EHU and 125 and 50 mV for the EDU represent a relatively high current density and a relatively low current density for each mode, respectively. Higher current densities are accompanied by higher decay rates, while lower reaction rates are much more stable. One possible reason may be mass transport limitations of the reactants and products.

In contrast to many other electrocatalytic systems using MEA architectures, the ACE/IPA EC-LOHC reactant and product are both liquids. Accordingly, both the reactant and the product liquids flow are diffusion-limited. While reactant depletion leads to lower reaction rates, product accumulation causes an unfavor-

able Nernst shift, leading to lower overpotentials within a given voltage hold. Both phenomena would manifest themselves in the form of a current decay.

The GDL materials used here are optimized for operating hydrogen fuel cells only. Therefore, GDL materials optimized for EC-LOHC operation could improve stability and yield higher current densities.

Furthermore, the decay rate at high current densities is noticeably lower for the EHU than for the EDU. This could reflect the aforementioned slow acetone (product) desorption. Because the EHU reduces acetone to isopropanol, an acetone affinity to the

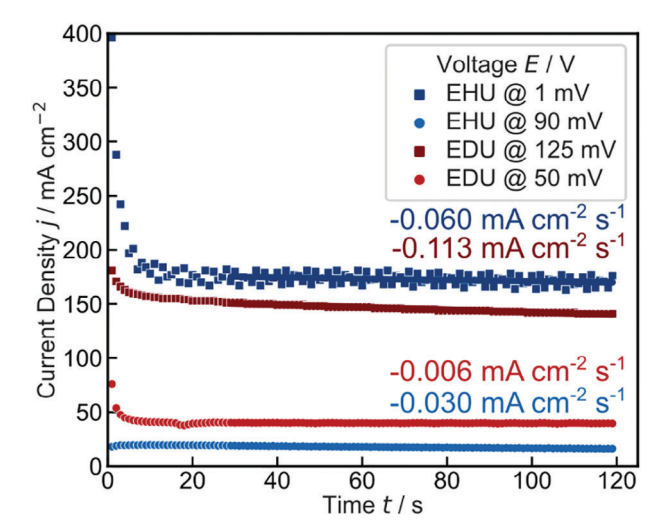


Figure 10. Representative raw data of a 2 min hold at varying voltages for the EHU using 1 M acetone and EDU using 1 M isopropanol at 50 °C. The given decay rates correspond to a linear fit slope between 31-120 s within 2 min hold. The bold line is the linear fit, comprising the used data points. The chosen holding points represent a point of relatively high current density and relatively low current density.

ADVANCED ENERGY MATERIALS

www.advenergymat.de

catalyst would not be harmful to the EHU but to the EDU. Optimized catalyst material could balance this acetone adsorption, yielding higher EDU stability.

Additionally, new membrane materials exhibiting low fuel crossover are vital to further increase the ACE/IPA concentration to improve the reaction rates or to lower the catalyst loadings.

Based on the results presented here and precisely because of the still-existing optimization potential, we see great prospects for this new hydrogen storage concept. We see the advantages of the EC-LOHC cycle in an application best utilized as stationary, seasonal energy storage for fluctuating renewable energies. A comparison of the EC-LOHC to existing energy storage technologies with economic advantages and disadvantages can be found in the Section \$10 (Supporting Information).

In conclusion, it must be emphasized that this work aims to present a new hydrogen storage concept that can compete with established technologies. However, because no long-term durability tests of this new concept have been carried out, the results must be seen as revealing the EC-LOHC's prospect and do not yet represent a life cycle analysis.

Nevertheless, we anticipate that the EC-LOHC concept can find substantial interest in various sustainable energy applications, exemplary for decentralized stationary seasonal storage of renewable energies for farms or in rural communities.

4. Conclusion

This work demonstrates the concept of a low-temperature acetone/isopropanol EC-LOHC for CO_2 emission-free hydrogen storage applications. The EC-LOHC consists of two processes that can be implemented by the EHU and the EDU, which can be operated in one PEM-MEA set-up, whereby the cell potential controls its direction. For $E < E_{rev}$ the cell is in the galvanic EHU mode, while for $E > E_{rev}$ the cell is in the electrolytic (electrolysis) EDU mode.

By investigating the influence of temperature, fuel concentrations, and different DoH on the polarization curves, considerable current densities in the range of 200 mA cm⁻² were achieved for both directions. Most observations for the polarization curves can be correlated to Nernst equation-related voltage dependencies, temperature-dependent reaction kinetics, and concentration-dependent fuel availability. Furthermore, the ionomer conductivity massively benefits from increased temperatures, while it decreases slightly with increasing organics concentrations. The results prove the endergonic dehydrogenation to be the EC-LOHC concept's limiting process. Overall, the corresponding reaction rates of the EDU are lower than for the EHU and are hampered to a greater extent by a product-shifted EC-LOHC-/EC-LOHC+ reaction equilibrium. The possible reason is a slow acetone desorption from the PtRu catalyst.

Based on the experimental results, we calculated efficiencies for PtP chains consisting of coupled water electrolysis and fuel cell systems. The storage efficiencies ($\eta_{Storage}$) for the acetone/isopropanol couple depend on the DoH reaction equilibrium and vary from 75 – 94 % for a DoH \geq 50 %, which is in the range of CH₂ and LH₂ and substantially better than thermocatalytic LOHC.

Possible material-related challenges currently lead to relatively high decay rates. However, further targeted research on corresponding optimized materials for this new concept can improve stability.

We encourage more research on this topic to improve this attractive EC-LOHC system presented here in an early yet already competitive state of development that appears highly attractive for stationary renewable energy storage.

5. Experimental Section

Membrane Electrode Assembly Manufacturing: PtRu/C (40/20 wt%, HISPEC 10 000, Alfa Aesar, USA) or Pt/C (40 wt.%, HISPEC4000, Alfa Aesar, USA), and Nafion D2021 (Chemours, USA) were dispersed in isopropanol (≥ 99.9 %, Merck KGaA, Germany) and water (18.2 MΩ, Merck-MilliPore, Germany) mixture (20/80) for 25 min at 40 W using an ultrasonic horn (UP200ST, Hielscher, Germany). The resulting catalyst inks had solid contents of 3 wt.% for PtRu/C and 1 wt.% for Pt/C, with 30 wt.% of the solid fraction being the ionomer. Subsequently, the catalyst ink was spray-coated on a gas diffusion layer (GDL) using an ExactaCoat (Sono-Tek Corporation, USA). PtRu/C inks were sprayed on an H23C2 GDL (Freudenberg & Co. KG, Germany), yielding a gas diffusion electrode (GDE) with a loading of 1 mg_{PtRu} cm^{-2} for the electrochemical hydrogenation of acetone and a loading of 2 $\rm mg_{PtRu}\,cm^{-2}$ for the electrochemical dehydrogenation of isopropanol. Pt/C inks were sprayed on an H23C8 GDL (Freudenberg & Co. KG, Germany), yielding a GDE with a loading of 0.3 mg_{Pt} cm⁻². After that, the corresponding PtRu/C GDE and a Pt/C GDE were hotpressed on a NafionXL membrane (27.5 µm thick e-PTFE reinforced Nafion membrane with incorporated chemical stabilizers^[94] by *Chemours*, USA) for 6 min at 155 °C and 120 N cm⁻² using a Labline P200S hotpress (COLLIN Lab & Pilot Solutions GmbH, Germany).

Cell Hardware and Test Set-Up: The electrochemical cell tests were performed using a Scribner (Scribner Associates Inc, USA) 850e testbench and Scribner cell fixture, including 5 cm² single serpentine graphite flow fields. The cell fixtures were tightened with a 5 Nm torque and the compression of the GDLs were adjusted with glass fiber reinforced PTFE gaskets (Hightech-flon, Germany) to 20–25 %. A Masterflex L/S peristaltic pump (Cole-Parmer, USA) fed the cell with the preheated organic reactant solutions. A VSP300 potentiostat (Biologic, France) was used to control the electrochemical measurements. (A depiction of the cell fixture, including a detailed description, is given in the Section S5, Supporting Information).

Electrochemical Measurements: The cell was heated to the desired temperature and fed with 5 mL min $^{-1}$ of the preheated reactant mixtures at the working electrode (organics side). The counter electrode (hydrogen side) was kept at 97 % relative humidity and ambient pressure and provided with 50 mL min $^{-1}$ hydrogen (5.0, Air Liquide, France) for the EHU or 1 L min $^{-1}$ 5 % H $_2$ in N $_2$ for the EDU. The 5 % H $_2$ gas was made by diluting 50 mL min $^{-1}$ H $_2$ and 950 ml min $^{-1}$ N $_2$ (5.0, Air Liquide, France).

In order to ensure pristine MEA states before each new set of experiments, the organic solvent side was flushed with DI water for at least 20 min with 5 mL min $^{-1}$ before each new experiment to clean leftover reactants and organics. The exact parameters for each experiment are in the Tables S2 and S3 (Supporting Information). Hydrogen crossover and ohmic short measurements were performed in a deoxygenated water/hydrogen (5 % $\rm H_2$ for EDU experiments) environment to monitor possible cell degradation throughout the experiment. The hydrogen crossover measurements were performed via voltage stepping (0.2 to 0.7 V in 0.1 V steps, hold time 2:30 min, and averaging the last 30 s). Linear regression was performed to obtain the electric short and the $\rm H_2$ crossover (Figure S2, Supporting Information; highest $\rm H_2$ crossover EHU: 1.07 mA cm $^{-2}$, EDU: 0.19 mA cm $^{-2}$; lowest electrical resistance EHU: 1.1 k $\rm \Omega$ cm 2 , EDU: 3.6 k $\rm \Omega$ cm 2).

ARR and IOR polarization characteristics were obtained using a mixed galvanostatic and potentiostatic protocol. The low current density regime of 1 – 10 mA cm $^{-2}$ was recorded galvanostatically. Because the catalyst's activity was potential dependent and to avoid unwanted side reactions, higher current densities were recorded potentiostatically. $^{[20,21]}$ The potentiostatic polarization curve points for the ARR were at 1, 5, 10, 20, 30, 40,

16146840, 2025, 12, Downloaded from https://advanced.onlinelibrary.wiley.com/doi/10.1002/aenm.202403824 by Forschungszentrum Jülich GmbH Research Center, Wiley Online Library on [09/042025]. See the Terms and Conditions (https://onlinelibrary.wiley

-and-conditions) on Wiley Online Library for rules of use; OA articles are governed by the applicable Creative Commons!

www.advancedsciencenews.com

www.advenergymat.de

50, 60, 70, 80, 90, and 100 mV. The potentiostatic polarization curve points for the IOR were at 25, 50, 75, 100, 125, 150, 175, 200, 225, 250, 275, and 300 mV. Each point was held for 2 min, while the last 30 s of each point were averaged for the data evaluation.

Electrochemical impedance spectroscopy (EIS) was measured for each polarization point from 100 kHz to 10 Hz with 10-30 % perturbation to determine the high-frequency resistances (HFR) using an equivalent circuit (inductor + resistor) with either a blocking-condition transmission line model^[96] or charge transfer transmission line model.^[97] All impedance spectra were fitted using the impedance.py library.^[98] Representative EIS raw data for the EHU and EDU is given in Figures S3 and S4 (Supporting Information).

Scope of the EHU and EDU Experiments: This study investigated the influence of temperature and fuel concentrations on the polarization curves and HFR of the electrochemical hydrogenation of acetone and the electrochemical dehydrogenation of isopropanol using a proton exchange membrane based membrane electrode assembly (PEM-MEA) set-up. All measurements were repeated three times each with an in-house produced MEA. The investigated temperature ranged from 30 - 70 °C, the acetone/isopropanol solutions varied from 0.1 - 2 M, and the mixed acetone/isopropanol solutions had a total organic concentration of 2 м. The complete data set, including HFR-free polarization curves and experimental parameters, is given in Figures S5–S11 (Supporting Information).

Supporting Information

Supporting Information is available from the Wiley Online Library or from the author.

Acknowledgements

The authors gratefully acknowledge the Bavarian Ministry of Economic Affairs, Regional Development and Energy for funding this work.

Open access funding enabled and organized by Projekt DEAL.

Conflict of Interest

The authors declare no conflict of interest.

Author Contributions

D.V. and A.M. contributed equally to this work. A.M. and D.V. conceived the concept, performed the experiments, evaluated the data, and wrote the manuscript. A.M. performed the EHU experiments. D.V. performed the EDU experiments. S.R. designed the PtP calculation and reviewed the manuscript. A.T.S.F. conceived the experimental concept, reviewed, and revised the manuscript. M.B. and M.W. reviewed the manuscript. P.W. conceived the concept, reviewed, revised the manuscript, and provided funding acquisition. S.T. conceived the concept, reviewed, and revised the manuscript, supervised the project, and provided funding acquisition. All the authors participated in the study discussion and approved the final version of the manuscript.

Data Availability Statement

The data that support the findings of this study are available from the corresponding author upon reasonable request.

Keywords

ec-lohc, electrocatalysis, electrochemical hydrogenation, electrochemical reforming, hydrogen storage, lohc

- [1] R. O'Hayre, S.-W. Cha, W. Colella, F. B. Prinz, Fuel Cell Fundamentals, 3rd ed., John Wiley and Sons, Hoboken, NJ 2016.
- [2] D. Berstad, S. Gardarsdottir, S. Roussanaly, M. Voldsund, Y. Ishimoto, P. Nekså, Renewable Sustainable Energy Rev. 2022, 154,
- [3] U. Cardella, L. Decker, J. Sundberg, H. Klein, Int. J. Hydrogen Energy 2017, 42, 12339.
- C. Hank, A. Sternberg, N. Köppel, M. Holst, T. Smolinka, A. Schaadt, C. Hebling, H.-M. Henning, Sustainable Energy Fuels 2020, 4, 2256.
- [5] M. Niermann, A. Beckendorff, M. Kaltschmitt, K. Bonhoff, Int. J. Hydrogen Energy 2019, 44, 6631.
- [6] P. Preuster, C. Papp, P. Wasserscheid, Acc. Chem. Res. 2017, 50, 74.
- [7] D. Teichmann, W. Arlt, P. Wasserscheid, Int. J. Hydrogen Energy 2012, 37, 18118.
- [8] D. Teichmann, W. Arlt, P. Wasserscheid, R. Freymann, Energy Environ. Sci. 2011, 4, 2767.
- [9] G. Sivakumar, R. Kumar, V. Yadav, V. Gupta, E. Balaraman, ACS Catal. 2023, 13, 15013.
- [10] V. Yadav, G. Sivakumar, V. Gupta, E. Balaraman, ACS Catal. 2021, 11, 14712
- [11] S. Giddey, S. P. S. Badwal, C. Munnings, M. Dolan, ACS Sustainable Chem. Eng. 2017, 5, 10231.
- [12] M. Bertau, H. Offermanns, L. Plass, F. Schmidt, H.-J. Wernicke, Methanol: The Basic Chemical and Energy Feedstock of the Future, Springer, Berlin, Heidelberg 2014.
- [13] L. Barelli, G. Bidini, G. Cinti, Energies 2020, 13, 6173.
- [14] V. Goyal, T. Bhatt, C. Dewangan, A. Narani, G. Naik, E. Balaraman, K. Natte, R. V. Jagadeesh, J. Org. Chem. 2023, 88, 2245.
- [15] M. Jitaru, J. Univ. Chem. Technol. Metall. 2007, 4, 333.
- [16] P. Gabrielli, M. Gazzani, M. Mazzotti, Ind. Eng. Chem. Res. 2020, 59,
- [17] K. Matsuoka, K. Miyoshi, Y. Sato, J. Power Sources 2017, 343, 156.
- [18] A. J. Bard, M. Stratmann, E. Gileadi, M. Urbakh, E. J. Calvo, P. R. Unwin, G. S. Frankel, D. D. Macdonald, P. Schmuki, S. Licht, F. Scholz, C. J. Pickett, H. J. Schäfer, G. S. Wilson, M. Fujihira, I. Rubinstein, J. F. Rusling, Encyclopedia of Electrochemistry, Wiley-VCH, Weinheim 2002-2007
- [19] J. Cho, B. Kim, S. Venkateshalu, D. Y. Chung, K. Lee, S.-I. Choi, J. Am. Chem. Soc. 2023, 145, 16951.
- [20] P. Khanipour, F. D. Speck, I. Mangoufis-Giasin, K. J. J. Mayrhofer, S. Cherevko, I. Katsounaros, ACS Appl. Mater. Interfaces 2020, 12, 33670.
- [21] I. Mangoufis-Giasin, O. Piqué, P. Khanipour, K. J. Mayrhofer, F. Calle-Vallejo, I. Katsounaros, J. Catal. 2021, 400, 166.
- [22] s. Supelco, Safety data Sheet Acetone, https://www.sigmaaldrich. com/DE/de/sds/mm/1.00014 (accessed: February 2024).
- [23] Carl Roth GmbH + Co KG, Safety-Data-Sheet: 2-Propanol, https://www.carlroth.com/medias/SDB-CN09-DE-DE.pdf?context= bWFzdGVyfHNIY3VyaXR5RGF0YXNoZWV0c3wzMDI0NTF8YXBwb GljYXRpb24vcGRmfGhjYi9oYTcvOTEzNzc5ODk3MTQyMi9TREJfQ0 4wOV9ERV9ERS5wZGZ8YWI3NjQ3NmJmOTJjZWFjNTZhYjU4YTIz MWE5MjA5OTZiNjFjMjMxY2E4Mzc2MTUyOGZjNDIwMTdmOTI1 N2ZkMg (accessed: February 2024).
- [24] C. J. Bondue, F. Calle-Vallejo, M. C. Figueiredo, M. T. M. Koper, Nat. Catal. 2019, 2, 243.
- [25] C. J. Bondue, Z. Liang, M. T. M. Koper, J. Phys. Chem. C 2021, 125,
- [26] Z. Liang, M. A. Villalba, M. T. Koper, Electrochim. Acta 2021, 391, 138911.

onditions) on Wiley Online Library for rules of use; OA articles are governed by the applicable Creative Commons!

ENERGY MATERIALS

www.advancedsciencenews.com

www.advenergymat.de

- [27] C. J. Bondue, M. Koper, J. Catal. 2019, 369, 302.
- [28] Y. Ando, T. Tanaka, M. Amano, Energy Convers. Manage. 2003, 44, 2811.
- [29] P. B. L. Chaurasia, Y. Ando, T. Tanaka, Int. J. Sustainable Energy 2007, 26, 107.
- [30] Y. Ando, Y. Aoyama, T. Sasaki, Y. Saito, H. Hatori, T. Tanaka, Bull. Chem. Soc. Jpn. 2004, 77, 1855.
- [31] S. K. Green, G. A. Tompsett, H. J. Kim, W. B. Kim, G. W. Huber, Chem-SusChem 2012, 5, 2410.
- [32] M. L. Perry, Z. Yang, J. Electrochem. Soc. 2019, 166, F3268.
- [33] C. Li, A. Sallee, X. Zhang, S. Kumar, Energies 2018, 11, 2691.
- [34] N. Kariya, A. Fukuoka, M. Ichikawa, Phys. Chem. Chem. Phys. 2006, 8, 1724.
- [35] C. Lamy, B. Guenot, M. Cretin, G. Pourcelly, Electrochim. Acta 2015, 177, 352.
- [36] F. M. Sapountzi, M. N. Tsampas, H. Fredriksson, J. M. Gracia, J. W. Niemantsverdriet, Int. J. Hydrogen Energy 2017, 42, 10762.
- [37] A. R. de La Osa, A. B. Calcerrada, J. L. Valverde, E. A. Baranova, A. de Lucas-Consuegra, Appl. Catal., B 2015, 179, 276.
- [38] C. Coutanceau, S. Baranton, WIREs Energy Environ. 2016, 5, 388.
- [39] B. Hasa, J. Vakros, A. Katsaounis, Mater. Today 2018, 5, 27337.
- [40] A. B. Calcerrada, A. R. de La Osa, J. Llanos, F. Dorado, A. de Lucas-Consuegra, Appl. Catal., B 2018, 231, 310.
- [41] E. R.-L. Angel Caravaca, P. Vernoux, F. Dorado, A. de Lucas-Consuegra, Chem. Eng. J. 2020, 396, 125217.
- [42] G. Sasikumar, A. Muthumeenal, S. Sundar Pethaiah, N. Nachiappan, R. Balaji, Int. J. Hydrogen Energy 2008, 33, 5905.
- [43] A. B. Calcerrada, A. R. de La Osa, A. Romero, J. L. Valverde, A. de Lucas-Consuegra, F. Dorado, J. Chem. Technol. Biotechnol. 2019, 94, 3698.
- [44] E. Ruiz-López, E. Amores, A. Raquel de la Osa, F. Dorado, A. de Lucas-Consuegra, Chem. Eng. J. 2020, 379, 122289.
- [45] M. Brodt, K. Müller, J. Kerres, I. Katsounaros, K. Mayrhofer, P. Preuster, P. Wasserscheid, S. Thiele, Energy Technol. 2021, 9, 2100164.
- [46] B. A. Santasalo, T. Kallio, K. Kontturi, Platin Met Rev. 2009, 53, 58.
- [47] A. Simanenko, P. K. Samal, R. Hübsch, J. Škvára, J. Yang, M. Kastenmeier, F. Winkler, T. Skála, N. Tsud, S. Mehl, J. Mysliveček, O. Brummel, Y. Lykhach, J. Libuda, ACS Energy Lett. 2024, 9, 4875.
- [48] P. Hauenstein, D. Seeberger, P. Wasserscheid, S. Thiele, *Electrochem. Commun.* **2020**, *118*, 106786.
- [49] P. Hauenstein, I. Mangoufis-Giasin, D. Seeberger, P. Wasserscheid, K. J. Mayrhofer, I. Katsounaros, S. Thiele, J. Power Sources Adv. 2021, 10, 100064.
- [50] S. Auffarth, W. Dafinger, J. Mehler, V. Ardizzon, P. Preuster, P. Wasserscheid, S. Thiele, J. Kerres, J. Mater. Chem. A 2022, 10, 17208.
- [51] D. Cao, S. H. Bergens, J. Power Sources 2003, 124, 12.
- [52] M. Minichová, C. van Pham, B. Xiao, A. Savan, A. Hutzler, A. Körner, I. Khalakhan, M. G. Rodríguez, I. Mangoufis-Giasin, V. Briega-Martos, A. Kormányos, I. Katsounaros, K. J. Mayrhofer, A. Ludwig, S. Thiele, S. Cherevko, *Electrochim. Acta* 2023, 444, 142032.
- [53] H. Kim, D. Kim, J. Son, S. Jang, D. Y. Chung, ACS Catal. 2024, 14, 8480.
- [54] P. Khanipour, M. Löffler, A. M. Reichert, F. T. Haase, K. J. J. Mayrhofer, I. Katsounaros, Angew. Chem., Int. Ed. 2019, 58, 7273.
- [55] National Institute of Standards and Technology, NIST: Isopropyl Alcohol, https://webbook.nist.gov/cgi/cbook.cgi?ID=C67630&Mask= 2#Thermo-Condensed (accessed: July 2024).
- [56] National Institute of Standards and Technology, NIST:Acetone, https://webbook.nist.gov/cgi/cbook.cgi?ID=C67641&Mask=2#Thermo-Condensed (accessed: July 2023).
- [57] M. W. Chase Jr., NIST-JANAF Themochemical Tables, 4th ed., American Institute of Physics, College Park, Maryland 1998, p. 1529.
- [58] J. D. Cox, D. D. Wagman, V. A. Medvedev, CODATA Key Values for Thermodynamics, Hemisphere Publishing Corp, New York 1984.

- [59] G. Zhang, S. G. Kandlikar, Int. J. Hydrogen Energy 2012, 37, 2412.
- [60] G. S. Harzer, A. Orfanidi, H. El-Sayed, P. Madkikar, H. A. Gasteiger, J. Electrochem. Soc. 2018, 165, F770.
- [61] Y. Wang, Y. Pang, H. Xu, A. Martinez, K. S. Chen, Energy Environ. Sci. 2022, 15, 2288.
- [62] Energy.gov, Technical Targets for Proton Exchange Membrane Electrolysis, https://www.energy.gov/eere/fuelcells/technical-targets-proton-exchange-membrane-electrolysis (accessed: September 2023).
- [63] H. L. O. H. C. Technologies, Hydrogenious LOHC Technologies, https://hydrogenious.net/how/#technology (accessed: July 2023).
- [64] K. Müller, S. Thiele, P. Wasserscheid, Energy Fuels 2019, 33, 10324.
- [65] E. Berretti, L. Osmieri, V. Baglio, H. A. Miller, J. Filippi, F. Vizza, M. Santamaria, S. Specchia, C. Santoro, A. Lavacchi, *Electrochem. Energy Rev.* 2023, 6, 30.
- [66] S. Z. S. Al Ghafri, A. Swanger, V. Jusko, A. Siahvashi, F. Perez, M. L. Johns, E. F. May, *Energies* 2022, 15, 1149.
- [67] D. I. Shishin, A. L. Voskov, I. A. Uspenskaya, Russ. J. Phys. Chem. 2010, 84, 1667.
- [68] A. S., Brunjes, M. J. P. Bogart, Ind. Eng. Chem. 1943, 35, 255.
- [69] O. A. Fedyaeva, E. G. Poshelyuzhnaya, Russ. J. Phys. Chem. 2017, 91,
- [70] D. Venus, M. Valeske, M. Brodt, P. Wasserscheid, S. Thiele, Electrochem. Commun. 2024, 169, 107823.
- [71] A. Caravaca, F. M. Sapountzi, A. de Lucas-Consuegra, C. Molina-Mora, F. Dorado, J. L. Valverde 2012, 37, 9504.
- [72] A. Rodríguez-Gómez, F. Dorado, A. de Lucas-Consuegra, A. R. de la Osa, Fuel Process. Technol. 2021, 222, 106954.
- [73] A. T. Pham, T. Baba, T. Shudo, Int. J. Hydrogen Energy 2013, 38, 9945.
- [74] S. Uhm, H. Jeon, T. J. Kim, J. Lee, J. Power Sources 2012, 198, 218.
- [75] K. C., Neyerlin, W., Gu, J. Jorne, H. A. Gasteiger, J. Electrochem. Soc. 2007, 154, 631.
- [76] J. Durst, A. Siebel, C. Simon, F. Hasche, J. Herranz, H. A. Gasteiger, Energy Environ. Sci. 2014, 7, 2255.
- [77] M. Bonanno, K. Müller, B. Bensmann, R. Hanke-Rauschenbach, D. Aili, T. Franken, A. Chromik, R. Peach, A. T. S. Freiberg, S. Thiele, Adv. Mater. Technol. 2024, 9, 2300281.
- [78] Z. Qi, A. Kaufman, J. Power Sources 2002, 110, 177.
- [79] A. Kusoglu, A. Z. Weber, Chem. Rev. 2017, 117, 987.
- [80] A. Buttler, H. Spliethoff, Renewable Sustainable Energy Rev. 2018, 82, 2440.
- [81] M. El-Shafie, Results Eng. 2023, 20, 101426.
- [82] S. A. Vilekar, R. Datta, J. Power Sources 2010, 195, 2241.
- [83] M. Moore, S. Shukla, S. Voss, K. Karan, A. Weber, I. Zenyuk, M. Secanell, J. Electrochem. Soc. 2021, 168, 044519.
- [84] M. Pourbaix, Atlas of Electrochemical Equilibria in Aqueous Solutions, National Association of Corrosion Engineers 1974.
- [85] S. Duerr, S. Zilm, M. Geisselbrecht, K. Mueller, P., Preuster, A. Bösmann, P. Wasserscheid, Int. J. Hydrogen Energy 2021, 46, 32583.
- [86] U. Eberle, M. Felderhoff, F. Schüth, Angew. Chem., Int. Ed. 2009, 48, 6608.
- [87] R. Folkson, Alternative Fuels and Advanced Vehicle Technologies for Improved Environmental Performance: Towards Zero Carbon Transportation, Woodhead Publishing, Sawston, Cambridge 2022.
- [88] F. Schüth, Eur. Phys. J. Spec. Top. 2009, 176, 155.
- [89] K. T. Møller, T. R. Jensen, E. Akiba, H. Li, Prog. Nat. Sci.: Mater. Int. 2017, 27, 34.
- [90] U. Cardella, L. Decker, H. Klein, Int. J. Hydrogen Energy 2017, 42, 13329.
- [91] U. Cardella, L. Decker, H. Klein, IOP Conf. Ser.: Mater. Sci. Eng. 2017, 171, 012013.
- [92] National Institute of Standards and Technology, Saturation Properties for Hydrogen Pressure Increments, https://webbook.nist.gov/cgi/fluid.cgi?Action=Load&ID=C1333740&Type=SatT&Digits=

16146840, 2025, 12, Downloaded from https://advanced.onlinelibrary.wiley.com/doi/10.1002/aenm.202403824 by Forschungszentrum Jülich GmbH Research Center,

Wiley Online Library on [09/04/2025]. See the Terms

www.advancedsciencenews.com

www.advenergymat.de

- 5&PLow=.5&PHigh=1.5&PInc=.1&RefState=DEF&TUnit=K&PUnit=atm&DUnit=kg/m3&HUnit=kJ/mol&WUnit=m/s&VisUnit=uPa<s&STUnit=N/m (accessed: January 2024).
- [93] K. Müller, K. Stark, V. N. Emel'yanenko, M. A. Varfolomeev, D. H. Zaitsau, E. Shoifet, C. Schick, S. P. Verevkin, W. Arlt, *Ind. Eng. Chem. Res.* 2015, 54, 7967.
- [94] S. Shi, A. Z. Weber, A. Kusoglu, J. Membr. Sci. 2016, 516, 123.
- [95] G. S. Harzer, J. N. Schwämmlein, A. M. Damjanović, S. Ghosh, H. A. Gasteiger, J. Electrochem. Soc. 2018, 165, F3118.
- [96] J. Landesfeind, J. Hattendorff, A. Ehrl, W. A. Wall, H. A. Gasteiger, J. Electrochem. Soc. 2016, 163, A1373.
- [97] R. Makharia, M. F. Mathias, D. R. Baker, J. Electrochem. Soc. 2005, 152, A970.
- [98] M. Murbach, B. Gerwe, N. Dawson-Elli, L. Tsui, JOSS 2020, 5, 2349.